IET Electric Power Applications

Research Article

IET Journals
The Institution of Engineering and Technology

Improve the performance characteristics of the IPMSM under the effect of the varying loads

ISSN 1751-8660
Received on 22nd February 2019
Revised 19th June 2019
Accepted on 1st July 2019
E-First on 2nd August 2019
doi: 10.1049/iet-epa.2019.0195
www.ietdl.org

Hamdy Mohamed Soliman[1] ✉

[1]*Department of Electrical Power and Machine Engineering, EL Marg High Institute for Engineering and Modern Technology, EL Marg, New EL Marg, Egypt*

✉ *E-mail: eldoctorhamdy70@gmail.com*

Abstract: Studying the dynamic performance is very important for improving the performance of the electrical machines. The sudden applied or removal the load is very critical for the electrical machines. It may lead to some problems in it's as, mechanical stress, surge current, increase the losses and decrease the motor life time. So, this paper studied this problem and constructed proposal model to reduce the effect of this problem on the electrical machines. This occurred through comparing between the effect of the dynamic load, sudden applied and removal loads on the performance characteristics of interior permanent synchronous motor (IPMSM) with proposal model and with classical model in the constant flux region and in the field weakening region. The simulation is done through the MATLAB program. The simulation shows the effectiveness of the proposal model on the performance characteristics of the IPMSM. With proposal model, the overshooting and under shooting of the motor speed are reduced. Rise time and settling time are improved, the response of the motor torque for load variations is improved and the stator currents are decreased. In this model, the space vector pulse width modulation is used to controlling the inverter which used to drive the IPMSM.

1 Introduction

Permanent magnet synchronous motor (PMSM) has become more popular for new drive systems. This motor replaces the induction motors and other motors in a wide application area. This is because it has many advantages such as high air gap flux density, high power factor, high acceleration and declaration rate, high torque-to-volume ratio, high torque per ampere, less maintenance, no commutation sparks due to no brushes, no rotor copper loss, high efficiency, compact structure and long-life time [1–5]. PMSMs have many types such as surface-mounted PMSM, inset PMSM, interior (buried) permanent magnet synchronous motor (IPMSM) and interior (buried) permanent magnet with circumferential synchronous motor [6]. Each type of them is called depending upon how the set adjusts the permanent magnet in or on the rotor of the motor. These PMSMs can be seen in Fig. 1.

The IPMSM is chosen in this article because it has many advantages compared to the other types of the PMSMs such as higher torque, higher air gap flux density, can be operated three times above the rated speed with less noise [7–9].

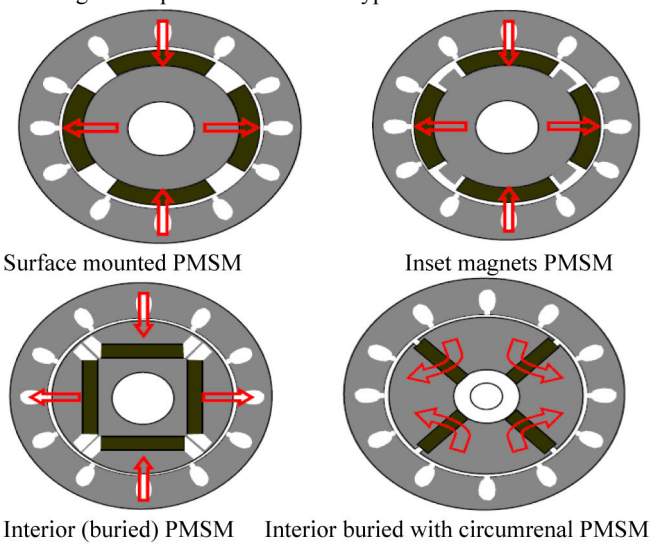

Fig. 1 *Different types of permanent magnet synchronous motor*

Despite these advantages of the IPMSM to get good performance, the precise of the motor control is very important. There are many modulation techniques to drive the IPMSM. These techniques can be classified into voltage control and current control. The voltage control mainly can be classified depending upon the type of the pulse width modulation. These classifications are six-step pulse width modulation, sinusoidal pulse width modulation and space vector pulse width modulation (SVPWM). For the current control methods, there are other techniques such as hysteresis current control, ramp control and delta modulation control. The current control techniques are simple and provide a faster response but have some disadvantages such as high ripple, high distortion, high harmonics at steady-state performance and high oscillation at transient performance. These problems can be overcome with voltage control, especially with the space vector modulation (SVM), so the SVPWM is used here.

In this article, the vector control with SVPWM is used to control the IPMSM in both the constant flux region and the field weakening region. A simple model is used to improve the performance characteristics of the IPMSM during the normal operation, dynamic operation and at sudden apply and removal of the load. Sudden change in the load, or in the field or harmonics increase in the motor torque may lead to hunting in the motor. This hunting leads to some impacts on the motor such as loss of synchronism, increase in the surge in the current, increase in the surge in the power flow, increase in the mechanical stress on the rotor shaft, increase in the motor losses, possibility of the resonance increase and motor temperature increase. To get rid of these problems, this paper suggested a simple model to reduce the effect of dynamic and sudden apply or removal of the load. The effect of this model can be seen in response to the motor speed and motor torque by observing the maximum overshooting, undershooting, the rise time and the settling time. This can also be seen in the shape of the current, the losses in the IPMSM and the performance overall. This paper can be divided into the following sections: introduction, mathematical model of IPMSM, vector control technique, the SVM, the proposed model, simulation results and conclusions.

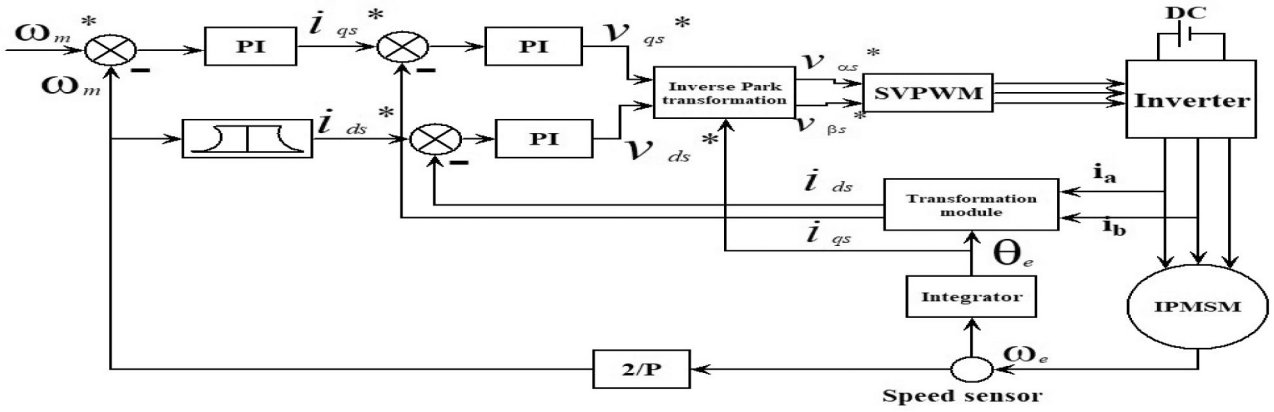

Fig. 2 *Classical vector control with SVPWM*

2 Mathematical model of IPMSM

The mathematical model of the IPMSM in the synchronous reference frame can be written as:

$$v_{ds} = R_s i_{ds} + L_d p i_{ds} - \omega_e L_q i_{qs} \tag{1}$$

$$v_{qs} = R_s i_{qs} + L_q p i_{ds} + \omega_e L_d i_{ds} + \omega_e \psi_f \tag{2}$$

$$T_m = \frac{3P}{4}[\psi_f i_{qs} + (L_d - L_q) i_{ds} i_{qs}] \tag{3}$$

$$J p \omega_m = T_m - T_L - \beta \omega_m \tag{4}$$

$$\omega_e = \frac{P}{2}\omega_m \tag{5}$$

$$\theta_e = \int \omega_e dt \tag{6}$$

where i_{ds}, i_{qs} are the d and q axes stator currents, v_{ds}, v_{qs} are the d and q axes stator voltages, L_d, L_q are the d and q axes stator inductances, R_s is the stator resistance per phase, T_m is the electromagnetic torque, T_L is the load torque, β is the friction coefficient for the motor, J is the moment of inertia, P is the number of poles of the motor, ω_e is the electrical frequency, ω_m is the mechanical motor speed, p is the differential operator and ψ_f is the rotor flux permanent magnet.

3 Vector control

Vector control is one of the methods used to control any AC motor. AC motor with the vector control method emulates the DC motor from the control side. This occurs by decoupling the stator current into torque and flux current components [10–17]. Fig. 2 shows how to apply the classical vector control on the IPMSM. To do this as shown in Fig. 2, the reference motor speed is compared to the actual motor speed and the error is introduced to the PI controller.

The output of this PI controller represents the quadrature component of the stator current in the synchronous reference frame. The other component of the stator current is deduced from the lookup table depending upon the value of the mechanical speed. The value of this current (direct axis stator current) is zero if the motor runs under or equal rated speed, at above rated speed this current will appear. These currents (direct and quadrature axes stator current) are compared to the transformation currents from the actual three-phase stator currents. These transformations occurred using Clark Park formulas. These transformations can be seen through (7) and (8), respectively. The transforming q-axis stator current is compared to the reference q-axis stator current and the error is introduced to another PI current controller to get the q-axis stator voltage. The transforming d-axis stator current is also compared to the reference d-axis stator current and the error is introduced to another PI current controller to get the d-axis stator voltage. These voltages with the help of rotor flux position are used to get two-axis stator voltage in the stationery reference frame. These stationery voltages are used to generate the pulses to drive the inverter through SVM block:

$$\begin{bmatrix} i_{\alpha s} \\ i_{\beta s} \end{bmatrix} = \begin{bmatrix} 1 & \frac{-1}{2} & \frac{-1}{2} \\ 0 & \frac{\sqrt{3}}{2} & \frac{-\sqrt{3}}{2} \end{bmatrix} \begin{bmatrix} i_a \\ i_b \\ i_c \end{bmatrix} \tag{7}$$

$$\begin{bmatrix} i_{ds} \\ i_{qs} \end{bmatrix} = \begin{bmatrix} \cos\theta_e & \sin\theta_e \\ -\sin\theta_e & \cos\theta_e \end{bmatrix} \begin{bmatrix} i_{\alpha s} \\ i_{\beta s} \end{bmatrix} \tag{8}$$

where i_a, i_b, i_c are the three-phase stator currents, and $i_{\alpha s}$, $i_{\beta s}$ are the α and β axes stator currents in the stationery reference frame.

4 Space vector pulse width modulation

To drive the IPMSM, the SVPWM technique is used. SVPWM is chosen because it has many advantages such as less harmonics, very fast response spatially during the transient performance and has a linear control range. SVPWM is used to generate some pulses. These pluses are used to drive the inverter. This occurs through controlling the switching of the inverter that reshaped the output voltages resulting from the inverter. During one switching period, the generating pulse is based on zero vectors and the switching between two adjacent active vectors. The switching state has eight states, which are six active states (V_1–V_6) and two non-active states (V_0 and V_7). The active states are shaped as a regular hexagon with the non-active state in the centre of the hexagon [18–20]. This regular hexagon is divided into six equal sectors. Each sector has a 60° dimension. The hexagon and the sectors can be seen in Fig. 3. Table 1 shows the switching states and the corresponding voltages. The line and phase voltages can be determined depending upon the switching state of the switching of the inverter. These voltages (line and phase voltages) can be determined as shown in (9) and (10), respectively:

$$\begin{bmatrix} v_{ab} \\ v_{bc} \\ v_{ca} \end{bmatrix} = v_{dc} \begin{bmatrix} 1 & -1 & 0 \\ 0 & 1 & -1 \\ -1 & 0 & 1 \end{bmatrix} \begin{bmatrix} a \\ b \\ c \end{bmatrix} \tag{9}$$

$$\begin{bmatrix} v_{an} \\ v_{bn} \\ v_{cn} \end{bmatrix} = \frac{v_{dc}}{3} \begin{bmatrix} 2 & -1 & -1 \\ -1 & 2 & -1 \\ -1 & -1 & 2 \end{bmatrix} \begin{bmatrix} a \\ b \\ c \end{bmatrix} \tag{10}$$

where v_{ab}, v_{bc}, v_{ca} are the three-phase line to line voltage, v_{an}, v_{bn}, v_{cn} are the three-phase line to neutral voltage, a, b, c are the operators to indicate the phase and v_{dc} is the input voltage of the inverter.

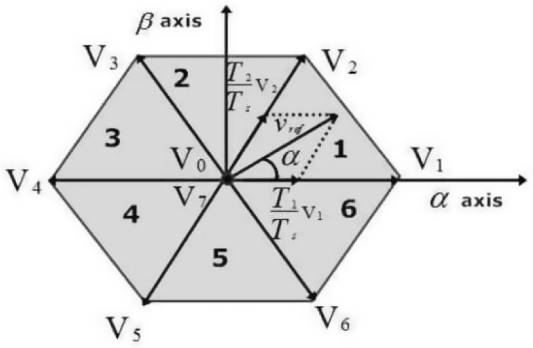

Fig. 3 *Inverter state (hexagon and sectors)*

Table 1 Switching state and the corresponding voltages

Voltage vector	Switching on	Line to neutral voltages			Line to line voltage		
		v_{an}	v_{bn}	v_{cn}	v_{ab}	v_{bc}	v_{ca}
V_0	T_1, T_3, T_5	0	0	0	0	0	0
V_1	T_2, T_3, T_5	2/3	−1/3	−1/3	1	0	−1
V_2	T_2, T_4, T_5	1/3	1/3	−2/3	0	1	−1
V_3	T_1, T_4, T_5	−1/3	2/3	−1/3	−1	1	0
V_4	T_1, T_4, T_6	−2/3	1/3	1/3	−1	0	1
V_5	T_1, T_3, T_6	−1/3	−1/3	2/3	0	−1	1
V_6	T_2, T_3, T_6	1/3	−2/3	1/3	1	−1	0
V_7	T_2, T_4, T_6	0	0	0	0	0	0

Table 2 Switching time for each switch

Sector	Upper switches	Lower switches
1	$s_1 = T_1 + T_2 + \frac{T_0}{2}, s_3 = T_2 + \frac{T_0}{2}, s_5 = \frac{T_0}{2}$	$s_2 = \frac{T_0}{2}, s_4 = T_2 + \frac{T_0}{2}, s_6 = T_1 + T_2 + \frac{T_0}{2}$
2	$s_1 = T_2 + \frac{T_0}{2}, s_3 = T_1 + T_2 + \frac{T_0}{2}, s_5 = \frac{T_0}{2}$	$s_2 = T_2 + \frac{T_0}{2}, s_4 = \frac{T_0}{2}, s_6 = T_1 + T_2 + \frac{T_0}{2}$
3	$s_1 = T_1 + T_2 + \frac{T_0}{2}, s_3 = T_2 + \frac{T_0}{2}, s_5 = \frac{T_0}{2}$	$s_2 = T_1 + T_2 + \frac{T_0}{2}, s_4 = T_2 + \frac{T_0}{2}, s_6 = \frac{T_0}{2}$
4	$s_1 = \frac{T_0}{2}, s_3 = T_2 + \frac{T_0}{2}, s_5 = T_1 + T_2 + \frac{T_0}{2}$	$s_2 = T_1 + T_2 + \frac{T_0}{2}, s_4 = T_2 + \frac{T_0}{2}, s_6 = \frac{T_0}{2}$
5	$s_1 = T_2 + \frac{T_0}{2}, s_3 = \frac{T_0}{2}, s_5 = T_1 + T_2 + \frac{T_0}{2}$	$s_2 = T_2 + \frac{T_0}{2}, s_4 = T_1 + T_2 + \frac{T_0}{2}, s_6 = \frac{T_0}{2}$
6	$s_1 = T_1 + T_2 + \frac{T_0}{2}, s_3 = \frac{T_0}{2}, s_5 = T_2 + \frac{T_0}{2}$	$s_2 = \frac{T_0}{2}, s_4 = T_1 + T_2 + \frac{T_0}{2}, s_6 = T_2 + \frac{T_0}{2}$

Depending upon the error between the reference axes of the stator current (i_{ds}^*, i_{qs}^*) and actual stator current after conversion to the synchronous reference frame (i_{ds}, i_{qs}), the reference voltages in the synchronous reference frame (v_{ds}^*, v_{qs}^*) can be generated through the two PI controllers. With the help of the rotor position, the reference voltages in the synchronous reference frame can be converted into the reference voltages in the stationery reference frame ($v_{\alpha s}^*, v_{\beta s}^*$). This transformation can be done as follows:

$$\begin{bmatrix} v_{\alpha s}^* \\ v_{\beta s}^* \end{bmatrix} = \begin{bmatrix} \cos\theta_e & -\sin\theta_e \\ \sin\theta_e & \cos\theta_e \end{bmatrix} \begin{bmatrix} v_{ds}^* \\ v_{qs}^* \end{bmatrix} \tag{11}$$

The reference voltages deduced from (11) are used to generate the pulses to drive the inverter for obtaining desired voltage to drive the IPMSM through the SVPWM block. To simulate the SVPWM, the following can be calculated

i. The reference voltage (v_{ref}) can be calculated as a vector depending upon the two-phase stationery reference frame voltages ($v_{\alpha s}^*, v_{\beta s}^*$) as in (12) and (13).
ii. The time duration (T_1, T_2, T_3) is calculated as in (15)–(17) for any sector.
iii. The switching time of each transistor ($S_1 - S_6$) is calculated depending upon (14)–(18) and as in Table 2.

4.1 Calculating the reference voltage

Depending upon the two reference voltages ($v_{\alpha s}$ and $v_{\beta s}$) in the stationery reference frame, the reference voltage as the vector can be calculated as:

$$v_{ref} = \sqrt{v_{\alpha s}^2 + v_{\beta s}^2} \tag{12}$$

$$\alpha = \tan^{-1}\frac{v_{\beta s}}{v_{\alpha s}} \tag{13}$$

4.2 Calculating the time duration

Depending upon Fig. 4 the time duration (T_1, T_2, T_s) in sector one can be calculated as in the following:

$$mv_{ref}\cos\alpha = \frac{T_1}{T_s}v_1 + \frac{T_2}{T_s}v_2\cos 60^\circ \tag{14}$$

$$mv_{\text{ref}}\sin\alpha = \frac{T_2}{T_s}v_2\sin 60^\circ \tag{15}$$

$$T_0 = T_s - (T_1 + T_2) \tag{16}$$

where m is the modulation index and T_S is the reciprocal of switching frequency.

To apply these times in each sector, the time duration can be written as:

$$T_1 = \frac{\sqrt{3}}{2}mT_s\sin\left(n\frac{\Pi}{3} - \alpha\right) \tag{17}$$

$$T_2 = \frac{\sqrt{3}}{2}mT_s\sin\left((n-1)\frac{\Pi}{3} - \alpha\right) \tag{18}$$

where n is the sector number.

4.3 Switching time for each switch

The switching time for each switch during the operation of the drive system can be seen in Table 2. It is very important to get good performance because it reshapes the output voltage from the inverter to control the motion of the IPMSM.

5 Proposal model

The overall stigmatic diagram for the proposal model can be seen in Fig. 5. This stigmatic diagram is as Fig. 2 add to its proposal block diagram. The proposal block diagram is used to readjust both the quadrature axis stator current and direct axis stator current as the reference to overcome the overshooting problems arising from any sudden variation or dynamic variation in the load. This occurs through calculating the load torque as in (19):

$$T_L = T_m - \beta\omega_m - Jp\omega_m \tag{19}$$

In this proposal model, a simple derivative model is used to generate the value of acceleration or deceleration during the load variation. This derivative depends upon the switching frequency. With the help of this derivative model, q-axis stator current and d-axis stator current (the transformation currents from actual three-phase current), the reference load torque is calculated. This reference load torque is introduced into the lookup table to get the stator current as of the magnitude. The use of this stator current depends upon the motor's working region e.g. constant flux region or field weakening region.

5.1 In constant flux region

In this region, the deducing current is taken as the q-axis stator current. This current is used to update the reference q-axis stator current. This q-axis reference current is the sum of deducing q-axis stator current from the lookup table and the q-axis stator current resulting from the output of the PI speed controller. The other component of the stator current (d-axis stator current) is also deduced from another lookup table depending upon the mechanical speed of the motor. The new reference controlling currents can be seen in Fig. 6. The new axis reference current is compared to the actual q-axis reference current and the error is introduced to the PI q-axis current controller to generate the reference q-axis voltage controller. The reference d-axis stator current is also compared to the actual d-axis stator current and the error is introduced to the PI d-axis current controller to generate the reference d-axis voltage

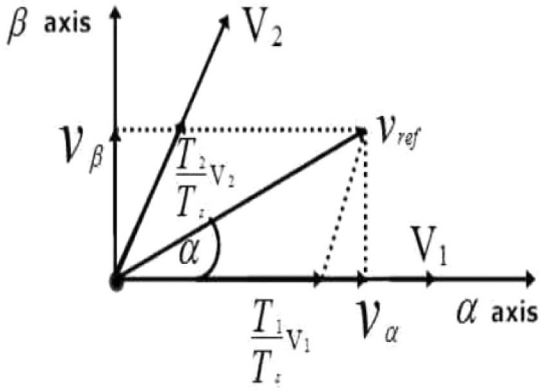

Fig. 4 *Voltage reference*

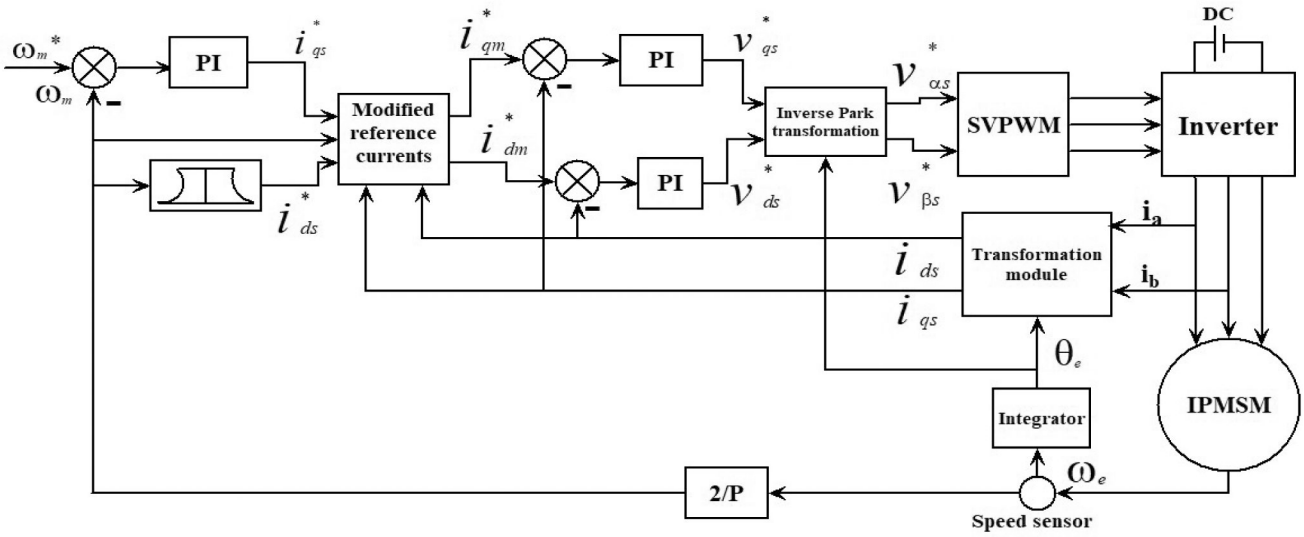

Fig. 5 *Proposal model to drive the IPMSM*

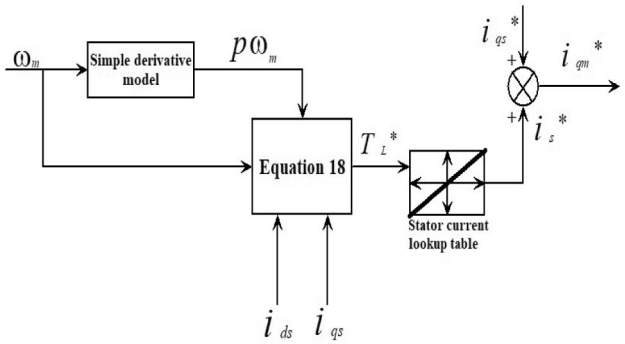

Fig. 6 *Modified reference current in constant flux region*

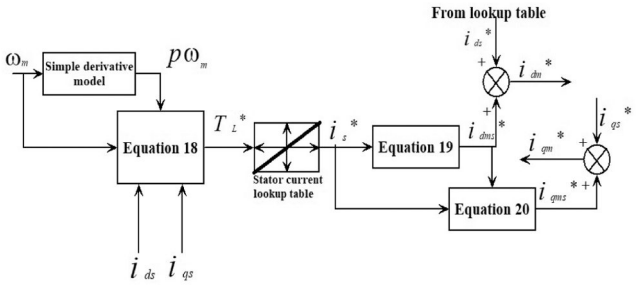

Fig. 7 *Modified reference currents*

Table 3 Motor data

Motor parameters	Values
power	720 W
voltage	380 V
motor speed	1700 rpm
poles	4
stator resistance	4.3 Ω
d-axis inductance	0.027 H
q-axis inductance	0.067 H
permanent magnet flux inductance	0.272 Wb
moment of inertia	0.000179 Kg.m^2

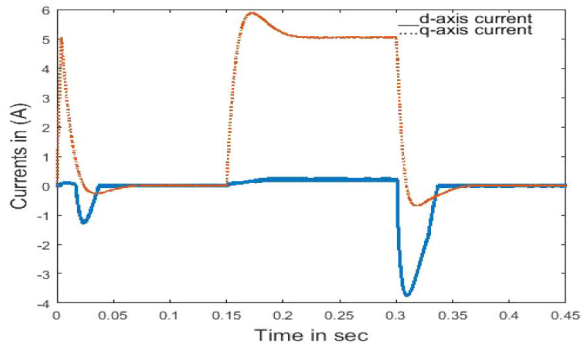

Fig. 8 *Variation of the d–q axes stator currents in the classical model*

controller. These voltages (*dq* voltages) with the help of rotor position is used to generate $\alpha - \beta$ voltages in the stationery reference frame. These voltages are introduced to the SVPWM block to generate the suitable pluses to drive the inverter. The output voltages from the inverter are applied to the motor to drive the motor. These driving voltages are used to reduce the effect of the variation in the load.

5.2 In field weakening region

If the motor runs above the rated speed, the stator current deducing from the lookup table of the load torque is divided into *d*-axis current component and *q*-axis current component. The *d*-axis current component can be written depending upon the relation which verifies the maximum torque per ampere [21–26]. This relation is in (20):

$$i_{d\text{ms}} = \frac{-\psi_\text{f} + \sqrt{\psi_\text{f}^2 + 4(L_d - L_q)^2 i_\text{s}^2}}{2(L_d - L_q)} \tag{20}$$

Also, the *q*-axis current component is in (21):

$$i_{q\text{ms}} = \sqrt{i_\text{s}^2 - i_{d\text{ms}}^2} \tag{21}$$

This *d*-axis current component is used to update the reference *d*-axis current with the help of *d*-axis current component that comes from the lookup table of the mechanical speed. The *q*-axis current component deducing from the proposal model is also used to update the reference *q*-axis current component with the help of the *q*-axis current component deducing from the PI speed controller. These modified reference currents can be seen in Fig. 7.

These reference currents (*dq* reference currents) are compared to the actual *dq* stator currents (the transformation currents from the actual three-phase stator currents by Park–Clark transformations) through the two PI controllers, one of them is used to deduce the *q*-axis reference voltage and the other is used to deduce the *d*-axis reference voltages. These deducing voltages are the primary voltages to generate the pluses which are used to drive the inverter to drive the IPMSM.

6 Simulation results

The load variations are simulated here. This is done in both the constant flux region and the field weakening region. The variation of the loads means sudden applied load, sudden removal load and gradually increasing and decreasing load. The effect of this variation is studied at the rated and the above rated frequencies. Two models are used: the classical model and the proposal model. This comparison between these models shows the effectiveness of the proposal model in both the constant flux region and the field weakening region. The motor parameters used in the simulation can be seen in Table 3.

6.1 Simulation in constant flux region

In this region, the effect of the load variations is studied at rated conditions with sudden applied load, removal load and dynamic load (gradually increasing load, gradually decreasing load and at load constant).

6.1.1 At rated frequency: At sudden apply and removal of the load: The impact of the sudden applied load and sudden removal of the load on the *d–q* axes stator currents can be seen here. The sudden load is applied for 0.15 s and sudden removal load is for 0.3 s in both models (classical and proposal). Figs. 8 and 9 show the variation of the *d–q* axes stator currents due to sudden apply and removal of the load. Fig. 8 shows the variation of the *d–q* axes stator currents in the classical model, while Fig. 9 shows the variation of the *d–q* axes stator currents in the proposal model. From these figures, it can be concluded that in the conventional model, there is a high sudden variation in the *d*-axis stator current when the load is removed and some simple variation in the *q*-axis stator current when the load is suddenly removed. At the sudden applied load, the *q*-axis stator current is not affected by this variation. In the proposal model, both the *d–q* axes stator currents are not affected by sudden apply or removal of the load and also the *d–q* axes stator currents reach the steady-state values faster than that their values in the classical model (Figs. 10 and 11).

The effect of sudden apply or removal of the load on the stator current can be neglected in the proposal model.

The motor torque versus the load torque can be seen in Figs. 12 and 13 in the classical and proposal models, respectively, where it is found that the motor torque in the proposal model is less effective by sudden apply or removal of the load and reaches the steady state faster compared to the classical model.

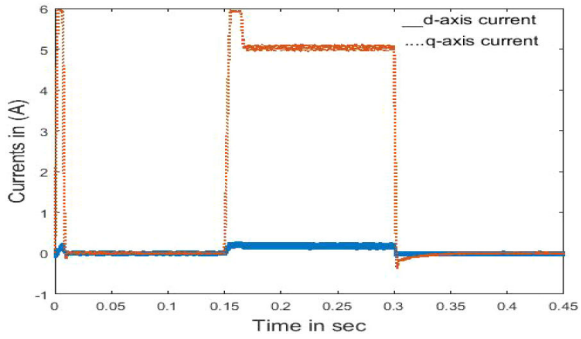

Fig. 9 *Variation of the d–q axes stator currents in the proposal model*

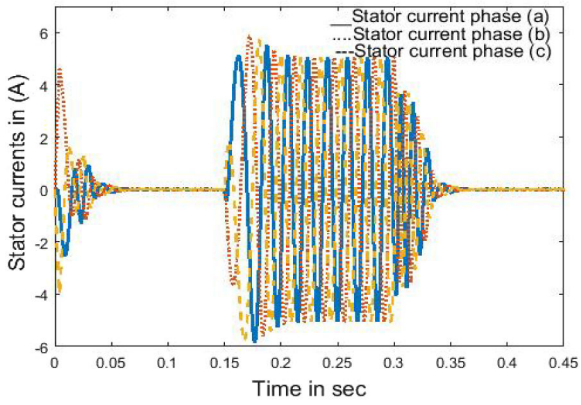

Fig. 10 *Variation of the stator current in the classical model*

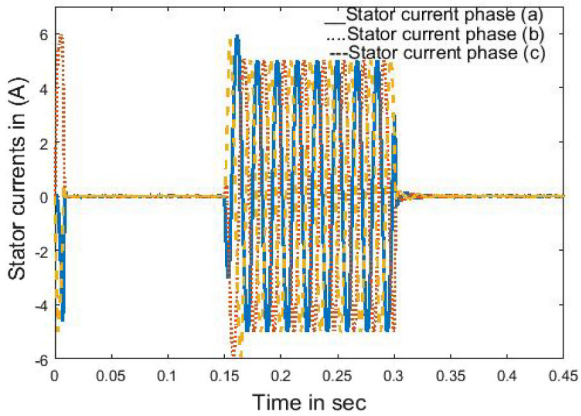

Fig. 11 *Variation of the stator current in the proposal model*

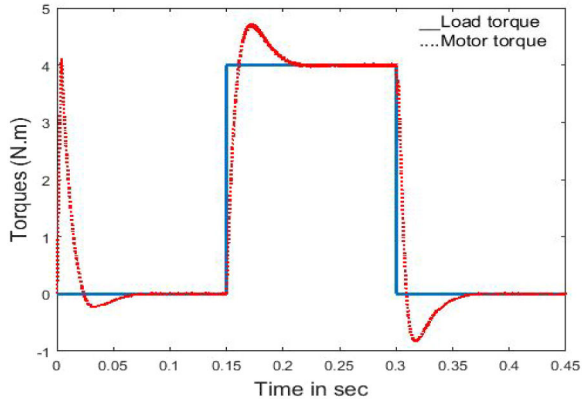

Fig. 12 *Response of the motor torques due to sudden apply and removal load torque in the classical model*

The effect of sudden apply and removal of the load on the motor speed can be seen in Figs. 14 and 15 in the classical and proposal models, respectively, where it is found that the motor

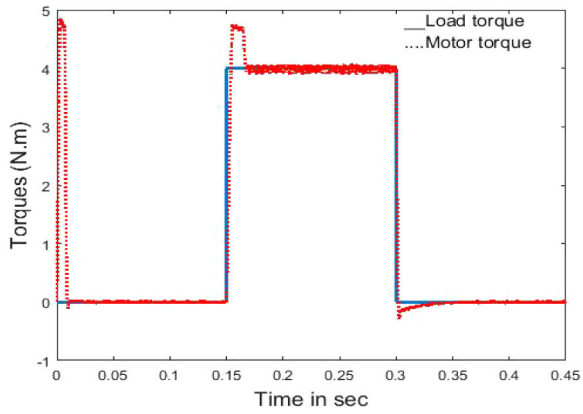

Fig. 13 *Response of the motor torques due to sudden apply and removal load torque in the proposal model*

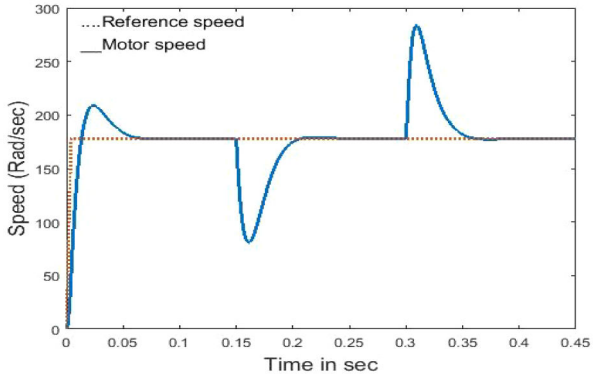

Fig. 14 *Variation of the motor speed due to sudden apply and removal load in the classical model*

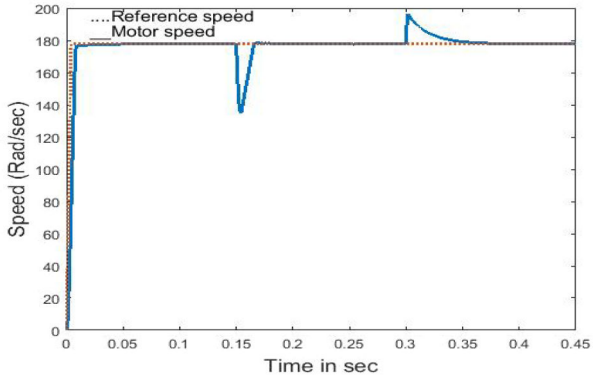

Fig. 15 *Variation of the motor speed due to sudden apply and removal load in the proposal model*

speed in the proposal model is less effective by sudden apply and removal of the load and reaches the steady state faster compared to the classical model. From these figures, it can also be concluded that the sudden load removal is more effective in the motor performance compared to the sudden applied load in the classical model.

To add more details on the motor performance, the following table shows the effect of the sudden apply and removal of the load on the motor speed with two methods under discussion. In this table, the rising time, settling time, over and under shooting are calculated where it is found that the rising time, settling time over and under shooting are improved in proposal model (Table 4).

At dynamic load: The load is applied and removed gradually. This load started from no load at 0 s and increased gradually and even reached the rated load torque at 0.1 s and continued with this load for up to 0.3 s, then the load decreased gradually and in 0.4 s. reached zero. The effect of these variations can be seen by studying the performance characteristics of the motor (IPMSM) in the classical and proposal models. Figs. 16 and 17 show the variation

Table 4 Dynamic response of IPMSM for two models in case of sudden removal load

Model type	Studying case	Rise time, s	Settling time, s	Maximum under-over shooting, %
classical model	Sudden applied load	0.0105	0.0125	−54
proposal model	—	0.007	0.0083	−22
classical model	Sudden removal load	0.363	0.383	160
proposal model	—	0.358	0.361	9

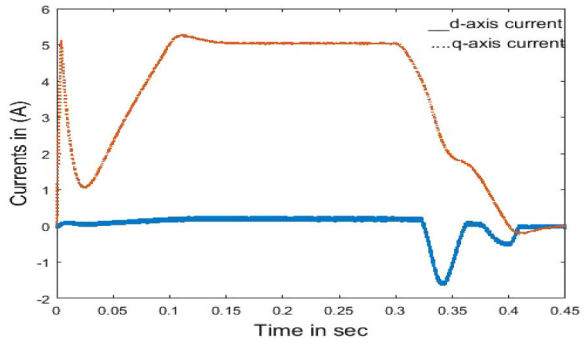

Fig. 16 *Variation of the d–q axes stator currents in the classical model*

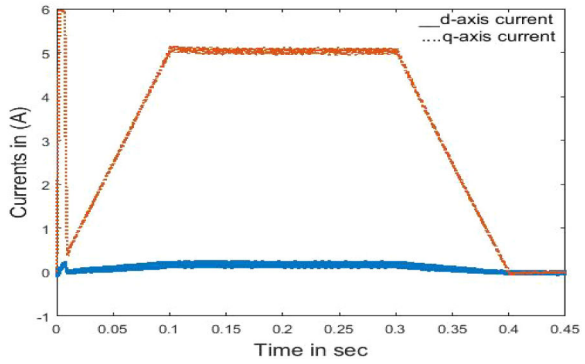

Fig. 17 *Variation of the d–q axes stator currents in the proposal model*

of the *d–q* axes stator currents due to the applied load and removal of this load. Fig. 16 shows the variation of the *d–q* axes stator currents in the classical model, while Fig. 17 shows the variation of the *d–q* axes stator currents in the proposal model. From these figures, it can be concluded that the removal load has more impact on the *d–q* axes stator currents in the classical model compared to the proposal model. The effect of load variations in the proposal model on the *d–q* axes of the stator currents can be neglected compared to the same impact in the classical model.

Figs. 18 and 19 show the effect of these variations of the load on the stator current where Fig. 18 shows the variation of the stator currents in the classical model due to variations of the load, while Fig. 19 shows the variation of the stator currents in the proposal model due to variation of the same load. From these figures, it can be concluded that the starting current is less in the proposal method. The stator current also shows less distortion in the proposal method compared to the classical model.

The motor torque versus the load torque can be seen in Figs. 20 and 21 in the classical and proposal models, respectively, where it is found that the motor torque is approximately congruent with load torque in case of the proposal model at increasing the load, at rated load and at decreasing the load and this did not occur in the classical model. This means that the proposal model is a very good model. The impact of the load variation on the motor speed can be seen in Figs. 22 and 23. This impact on the motor speed in the classical model can be seen in Fig. 22, while this impact on the

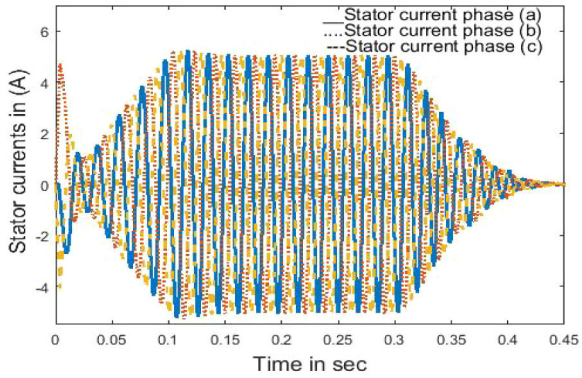

Fig. 18 *Variation of the stator current in the classical model*

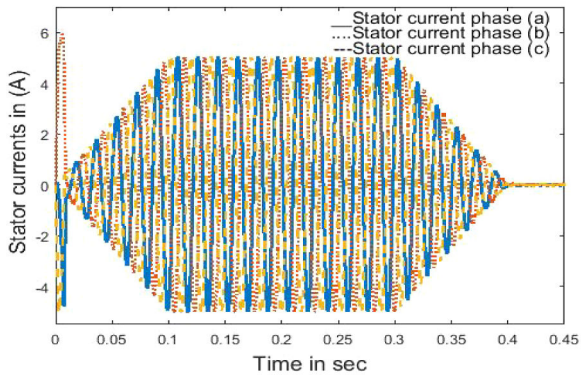

Fig. 19 *Variation of the stator current in the proposal model*

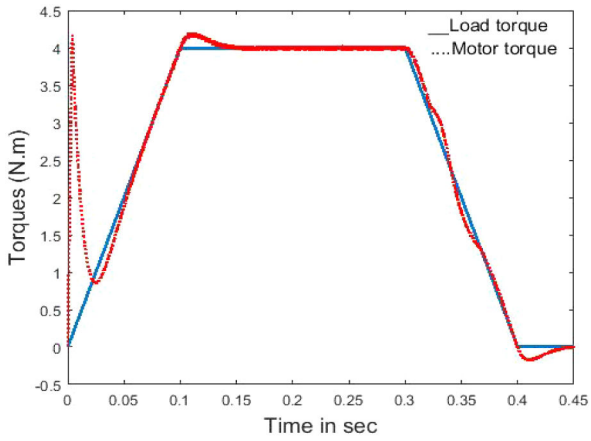

Fig. 20 *Response of the motor torques with load torque in the classical model*

motor speed in the proposal model can be seen in Fig. 23. From these figures, it can be concluded that the variation of the motor speed can be neglected in case of load variations in the proposal model compared to the classical model. Where it can be concluded that the classical model shows more reaction with this variation in the load.

6.2 Simulation in field weakening region

In this region, the effect of the load variations is studied. The motor speed increased to one and half of the rated speed, and also the load decreased to half of the rated value.

6.2.1 At one and half of the rated frequency: At sudden apply and removal of the load: The effect of sudden apply and removal of the load on the *d–q* axes stator currents can be seen here. The sudden applied load is for 0.15 s and sudden removal of the load is for 0.3 s in both models. Figs. 24 and 25 show the variation of the *d–q* axes stator currents due to the sudden applied load and sudden removal of the load in the classical and proposal models,

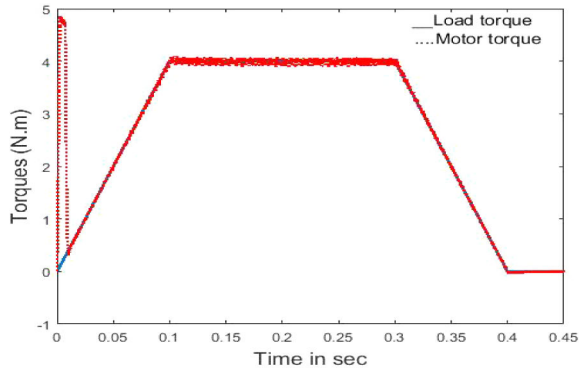

Fig. 21 *Response of the motor torques with load torque in the proposal model*

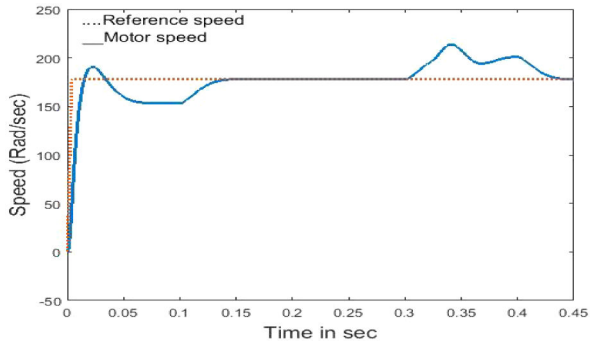

Fig. 22 *Variation of the motor speed with load variation in the classical model*

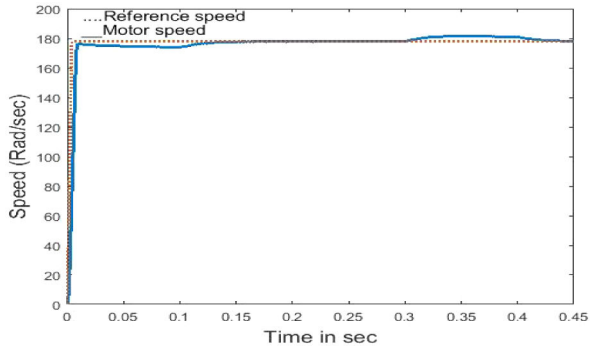

Fig. 23 *Variation of the motor speed with load variation in the proposal model*

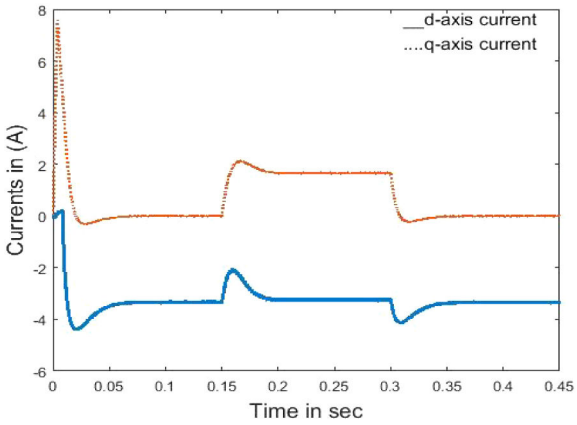

Fig. 24 *Variation of the d–q axes stator currents in the classical model*

respectively. From these figures, it can be concluded that a high sudden variation occurs on the *d–q* axes stator currents when the load is suddenly applied or suddenly removed in the conventional model compared to the proposal model. The *d–q* axes stator currents are high at the start in the conventional model compared to

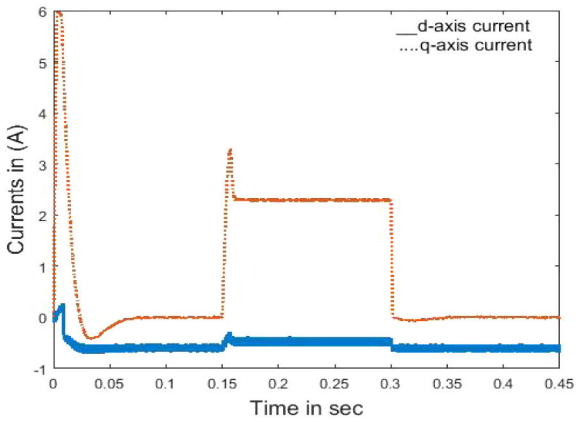

Fig. 25 *Variation of the d–q axes stator currents in the proposal model*

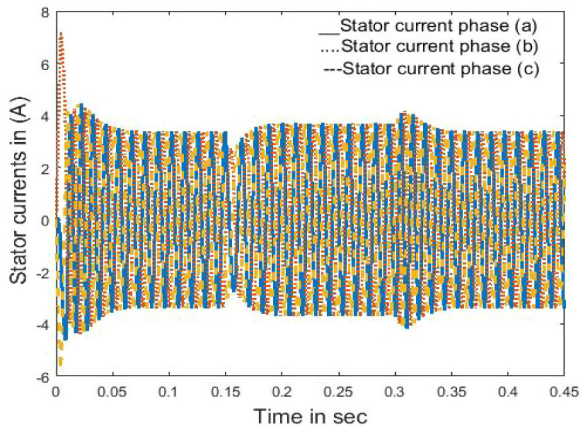

Fig. 26 *Variation of the stator current in the classical model*

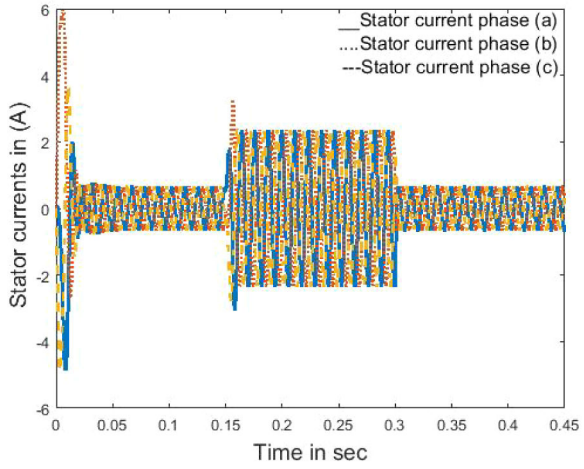

Fig. 27 *Variation of the stator current in the proposal model*

the proposal model. With sudden removal of the load, the *d*-axis stator current is still high in the classical model compared to the proposal model.

The effect of sudden apply and removal of the load on the stator current in the classical and proposal models can be seen in Figs. 26 and 27, respectively, where it is found that in the proposal model, the stator currents decreased at the start at loading and at sudden removal load but these currents were higher in the classical model. This means that the copper losses increased and the efficiency decreased in the classical model.

The motor torque versus the load torque can be seen in Figs. 28 and 29 in the classical and proposal models, respectively, where it is found that the motor torque in the proposal model is less effective with sudden apply or removal of the load and reached the steady state faster compared to the classical model.

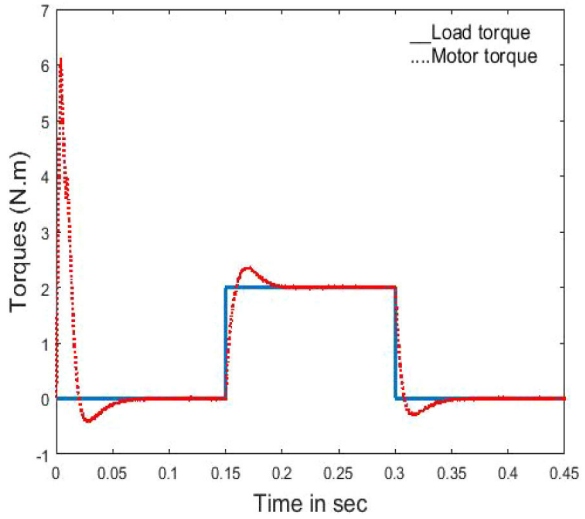

Fig. 28 *Response of the motor torques due to sudden apply and removal load torque in the classical model*

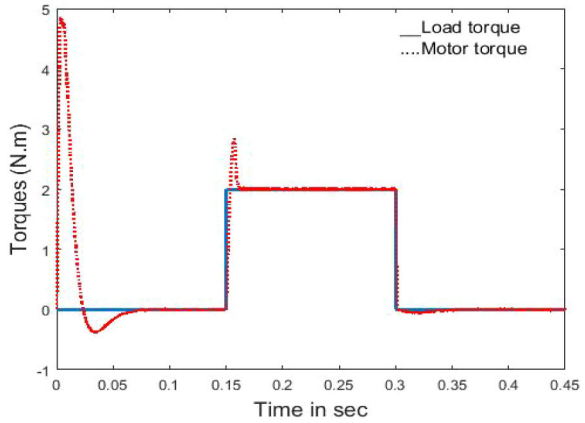

Fig. 29 *Response of the motor torques due to sudden apply and removal load torque in the proposal model*

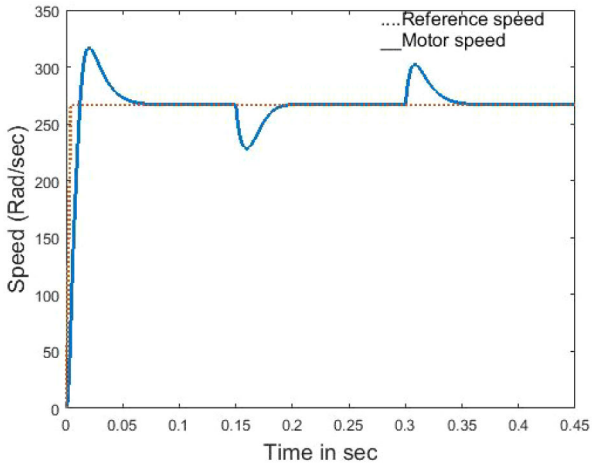

Fig. 30 *Variation of the motor speed due to sudden apply and removal load in the classical model*

The effect of sudden apply and removal of the load on the motor speed can be seen in Figs. 30 and 31 in the classical and proposal models, respectively, where it is found that the motor speed in the proposal model is less effective with sudden apply and removal of the load and reached the steady state faster compared to the classical model. From these, it can be concluded that the motor speed is above rated because the motor is working in the field weakening region.

At dynamic load: The load is applied and removal gradually. This load started from no load at 0 s and increased gradually and

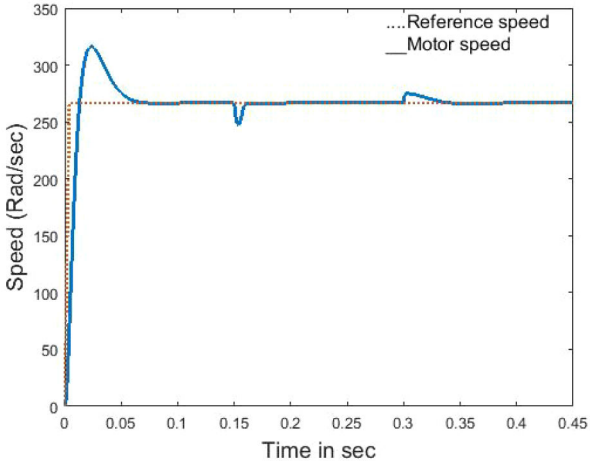

Fig. 31 *Variation of the motor speed due to sudden apply and removal load in the proposal model*

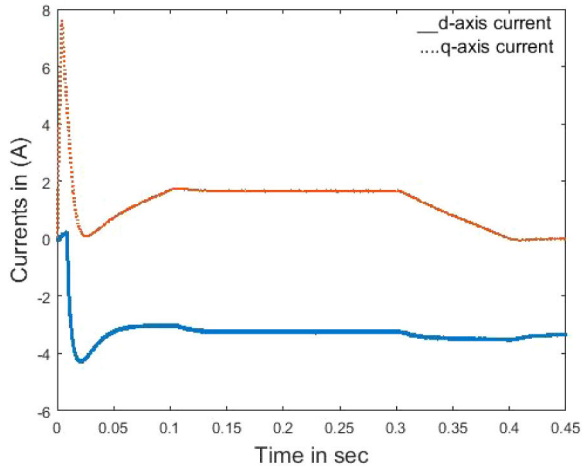

Fig. 32 *Variation of the d–q axes stator currents in the classical model*

even reached the rated load torque at 0.1 s and continued with this load for up to 0.3 s, then the load decreased gradually and in 0.4 s reached zero. The effect of these variations can be seen by studying the performance characteristics of the motor (IPMSM) in the classical and proposal models. Figs. 32 and 33 show the variation of the *d–q* axes stator currents due to applied load and removal of this load. Fig. 32 shows the variation of the *d–q* axes stator currents in the classical model, while Fig. 33 shows the variation of the *d–q* axes stator currents in the proposal model. From these figures, it can be concluded that the *d–q* axes stator current is higher in the classical model in case of gradually increasing the load and gradually decreasing the load and also at constant load, but in the proposal model, these currents decreased. The variation of the stator currents in the classical and proposal models can be seen in Figs. 34 and 35, respectively, where it is found that in the proposal model, the stator currents decreased at the start at constant loading and at gradually increasing or decreasing the load, but these currents are higher in the classical model. This means that the copper losses increased and the efficiency decreased in the classical model.

The motor torque versus the load torque can be seen in Figs. 36 and 37 in the classical and proposal models, respectively, where it is found that the motor torque showed more improvement in the proposal model compared to the classical model.

The effect of the load variation on the motor speed can be seen in Figs. 38 and 39 which showed more improvement in the proposal model compared to the classical model.

7 Conclusion

The impact of the load variations on the performance characteristics of the IPMSM is studied in this paper. This occurred

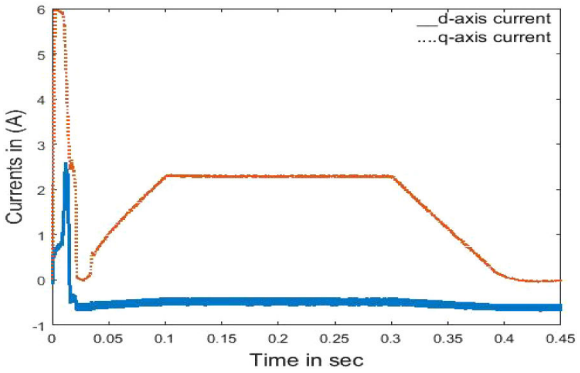

Fig. 33 *Variation of the d–q axes stator currents in the proposal model*

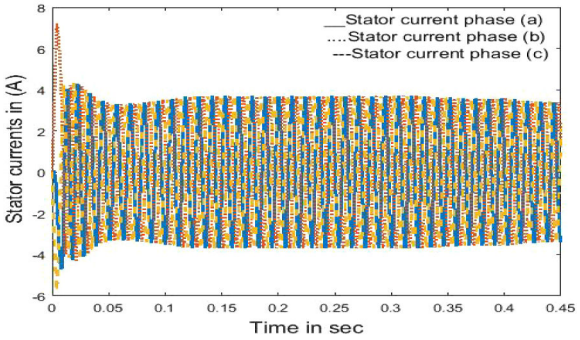

Fig. 34 *Variation of the stator current in the classical model*

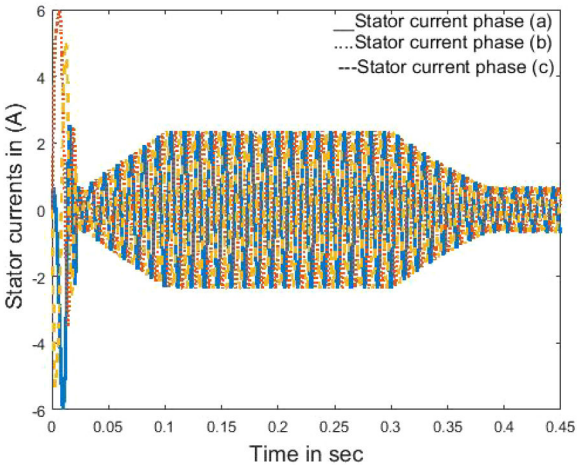

Fig. 35 *Variation of the stator current in the proposal model*

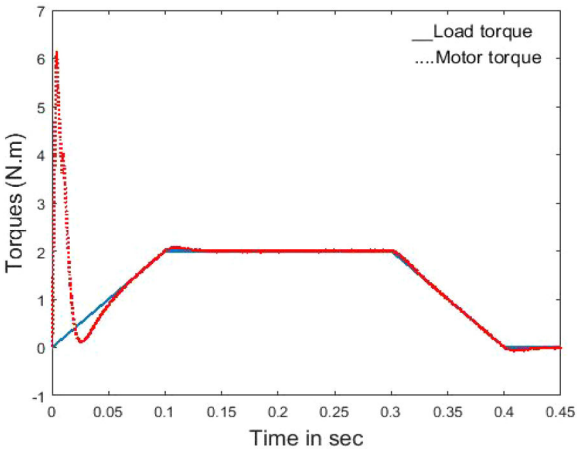

Fig. 36 *Motor torques versus load torque in the classical model*

in the constant flux region and in the field weakening region at sudden applied load, at sudden removal load, at gradually

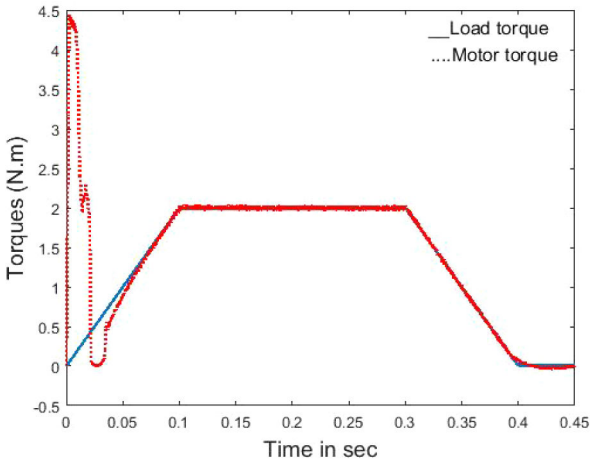

Fig. 37 *Motor torques versus load torque in the proposal model*

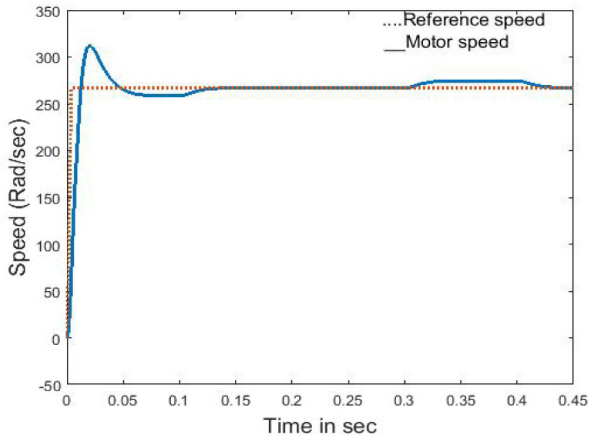

Fig. 38 *Variation of the motor speed due to sudden apply and removal load in the classical model*

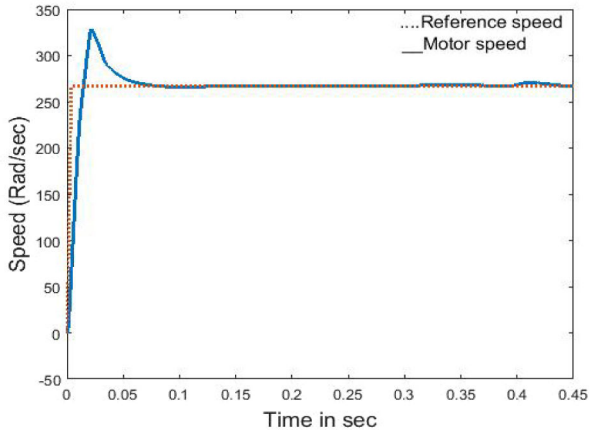

Fig. 39 *Variation of the motor speed due to sudden apply and removal load in the proposal model*

increasing load, at gradually decreasing load and at load constant. The vector control with SVPWM is used due to the advantages of this method. The proposal model is constructed to improve the performance characteristics of the IPMSM during the load variations. This model is compared to the classical model to show the effect of this on the performance of the IPMSM. The simulation proved that all the performance characteristics of the IPMSM showed improvement in the proposal model compared to the classical model.

8 References

[1] Smith, T., Jones, M.: 'Model predictive control of induction motor drives: torque control versus flux control', *IEEE Trans. Ind. Appl.*, 2016, **52**, (5), pp. 4050–4060

[2] Xu, Y., Shi, T., Yan, Y.*, et al.*: 'Dual-vector predictive torque control of permanent magnet synchronous motors based on a candidate vector table', *Energies*, 2019, **12**, (1), pp. 1–15

[3] Kar, N.C., Hamidifar, S., Kazerooni, M: 'Analytical modelling and parametric sensitivity analysis for the PMSM steady-state performance prediction', *IET Electr. Power Appl.*, 2013, **7**, (7), pp. 586–596

[4] Younesi, A., Tohidi, S., Feyzi, M.R.: 'Improved optimization process for nonlinear model predictive control of PMSM', *Iran. J. Electr. Electron. Eng.*, 2018, **14**, (3), pp. 278–288

[5] Karunamoorthy, B., Dhivyaa, D.: 'Design of PMSM and its application', *Int. J. Curr. Res.*, 2017, **9**, (5), pp. 51047–51050

[6] El-Refaie, M., Jahns, T. M.: 'Comparison of synchronous PM machine types for wide constant-power speed range operation'. Conf. Rec. 14th IEEE IAS Annu. Meeting, Hong Kong, 2005, vol. 2, pp. 1015–1022

[7] Soleimani, J., Vahedi, A., Mirimani, S.M.: 'Inner permanent magnet synchronous machine optimization for HEV traction drive application in order to achieve maximum torque per ampere paper', *Iran. J. Electr. Electron. Eng.*, 2011, **7**, (4), pp. 241–248

[8] Noguchi, T.: 'Trends of permanent-magnet synchronous machine drives', *Trans. Electr. Electron. Eng.*, 2007, **2**, pp. 125–142

[9] Pellegrino, G., Vagati, A., Guglielmi, P.*, et al.*: 'Performance comparison between surface-mounted and interior PM motor drives for electric vehicle application', *IEEE Trans. Ind. Electron.*, 2012, **59**, (2), pp. 803–811

[10] Vishwakarma, P.K.: 'Design and simulation vector control of permanent magnet synchronous motor', *Int. J. Sci. Res. & Dev.*, 2018, **6**, (4), pp. 1327–1331

[11] Liu, T., Chen, G., Li, S.: 'Application of vector control technology for PMSM used in electric vehicles paper', *Open Autom. Control Syst. J.*, 2014, **6**, pp. 1334–1341

[12] Konghirun, M., Xu, L.: 'A *dq*-axis current control technique for fast transient response in vector controlled drive of permanent magnet synchronous motor'. The 4th Int. Power Electronics and Motion Control Conf. IPEMC-2004, IEEE Conf. Publications, Xi'an, People's Republic of China, 2004, pp. 1316–1320

[13] Espina, J., Arias, A., Balcells, J.*, et al.*: 'Speed anti-windup PI strategies review for field oriented control of permanent magnet synchronous machines'. Compatibility and Power Electronics CPE-2009, IEEE Conf. Publications, Badajoz, Spain, 2009, pp. 279–285

[14] Zhang, J.S.: 'Matlab-based permanent magnet synchronous motor vector control simulation'. Proc. of the 2010 3rd IEEE Int. Conf. on Computer Science and Information technology, Chengdu, People's Republic of China, July 2010, pp. 539–542

[15] Madhu, R.K., Mathew, A.: 'Matlab/simulink model of field oriented control of pmsm drive using space vectors', *Int. J. Adv. Eng. Technol.*, 2013, **6**, (3), pp. 1355–1364

[16] Morel, F., Lin-Shi, X.F., Retif, J.M.: 'A comparative study of predictive current control schemes for a permanent-magnet synchronous machine drive', *IEEE Trans. Ind. Electron.*, 2009, **56**, (7), pp. 2715–2728

[17] Yang, S.M., Lin, K.W.: 'Automatic control loop tuning for permanent-magnet AC servo motor drives', *IEEE Trans. Ind. Electron.*, 2016, **63**, (3), pp. 1499–1506

[18] Liu, X., Gu, Z., Zhao, J.: 'Torque ripple reduction of a novel modular arc-linear flux-switching permanent magnet motor with rotor step skewing', *Energies*, 2016, **9**, pp. 1–15

[19] Kumar, P., Lakra, D., Makin, R.: 'Modeling and simulation of field oriented control PMSM drive system using SVPWM technique', *Int. J. Eng. Trends Technol.*, 2016, **39**, (4), pp. 184–188

[20] Singh, N.K., Tiwari, P.: 'Enhancing stability & performance analysis of PMSM using SVPWM & PI controller', *Int. J. Sci. Eng. Technol. Res.*, 2016, **5**, (5), pp. 1429–1433

[21] Bariša, T, Sumina, D, Kutija, M.: 'Comparison of maximum torque per ampere and loss minimization control for the interior permanent magnet synchronous generator', Int. Conf. on Electrical Drives and Power Electronics, Tatranska Lomnica, Slovakia, 2015, pp. 497–502

[22] Wang, M.-S., Hsieh, M.-F., Syamsiana, I.N.*, et al.*: 'Fuzzy maximum torque per ampere and maximum torque per voltage control of interior permanent magnet synchronous motor drive', *Sens. Mater.*, 2017, **29**, (4), pp. 461–472

[23] Sumesh, M., Helen, S., Kavitha, M.*, et al.*: 'Implementation of maximum torque per ampere algorithm in PMSM', *Int. J. Eng. Sci. Comput.*, 2016, **6**, (3), pp. 2533–2538

[24] Hoang, K.D., Aorith, H.K.A.: 'Control of IPMSM drives for traction applications considering machine parameter and inverter nonlinearities', *IEEE Trans. Transp. Electrification*, 2015, **1**, (4), pp. 312–325

[25] Sun, T., Wang, J., Koc, M.*, et al.*: 'Self-learning MTPA control of interior permanent-magnet synchronous machine drives based on virtual signal injection', *IEEE Trans. Ind. Appl.*, 2016, **52**, (4), pp. 3062–3070

[26] Songa, Q., Jiaa, C.: 'Robust speed controller design for permanent magnet synchronous motor drives based on sliding mode control', *Energy Proc.*, 2016, **88**, pp. 867–873